IMPACT OF CONFORMAL COATING INDUCED STRESS ON WAFER LEVEL CHIP SCALE PACKAGE THERMAL CYCLING PERFORMANCE

[1]Andy Hsiao, [1]Mohamed Sheikh, [2]Karl Loh, [2]Edward Ibe, and [1]Tae-Kyu Lee
[1]Portland State University, Portland, OR
[2]Zymet, East Hanover, NY

ABSTRACT

Conformal coating is commonly used for harsh environment to protect electronics from moisture and chemical contaminants. But the stresses imparted by the conformal coating can cause degradation to the package thermal cycle performance. Full coverage of the component with conformal coating material can prevent potential corrosion induced degradation but imply a local compression stress during thermal cycling, resulting a different thermal cycling performance compared to non-coated components. In this study, 8x8mm^2 wafer level chip scale packages (WLCSP) were subjected to 5% NaCl aqueous spray test with and without full conformal coating, then thermal cycled from -40ºC to +125ºC. Weibull reliability statistics indicated that fully conformal coated components experience characteristic life cycle number reduction from 404 cycles to 307 cycles, a 24% lifetime reduction, comparing to no conformal coated, no salt spray test applied components. The correlation between crack propagation and localized recrystallization were compared in a series of cross section analyses using polarized imaging and electro-backscattered diffraction (EBSD), which revealed that the conformal coating induced a z-axis tension and compression strain during thermal cycling, resulting in an accelerated degradation at the solder interconnect. Linear Laser profilometer measurements showed that fully conformal coated samples experienced a higher z-axis height displacement change relative to non-conformal coated samples when exposed to 125°C with 10 minutes dwell. To prevent this z-axis strain a reworkable edgebond adhesive was applied with full conformal coating configuration, which demonstrate an increase of characteristic lifecycle number to 2783 cycles, suggesting that the mitigation of the z-axis strain can vastly enhance the thermal cycling performance.

Keywords: WLCSP, Conformal coating, thermal cycling, microstructure

INTRODUCTION

The need for corrosion resistance performance in electronic devices and components become more important with emerging applications in wide range of environments subjected to a diverse array of extreme conditions [1-3]. The amount of data concerning the corrosion properties of electronic products are continuously growing. It is well established that tin-based interconnections like solder joints are less problematic subjected to corrosion because of their relatively strong corrosion resistance.[4-6] It has been reported that the main component of solder alloys, tin (Sn), resists corrosion because of the passivity of the film that forms on its surface [7,8]. The results of various studies show that Sn–3.0Ag–0.5Cu (wt%) (SAC305) solder exhibits better corrosion resistance than other Sn-based alloy compositions due to its high content of noble or inert elements (Ag and Cu) and its stable structure [7,9]. But in earlier publication, it was also shown that the existence of Cu_6Sn_5 and Ag_3Sn intermetallic precipitates in the solder provided unique conditions to the solder joint corrosion mechanism [4,10]. These intermetallic precipitates, in addition to functioning as noble materials, also form galvanic couples with the Sn. Even though the NaCl condition did not affect the whole Sn based solder joint, a localized reaction can degrade the joint stability. Also the NaCl solution did not degrade all solder joints but affected selected joints which are preferred in grain orientation [10]. Figure 1 shows the correlation between the corrosion path and the c-axis direction of the Sn lattice after solder joints after 5% NaCl test. It revealed that the Corrosion path affected by just a small portion of corrosion region at the initiation point then with crack propagation followed and aligned with the Sn lattice basal plane [10]. Given this example, even if the overall solder joint did not experience severe corrosion, it shows that the joint can suffer accelerated thermal fatigue crack initiation due to the brittle nature of the oxide phase at the stress concentration point. Thus, preventing such localized corrosion in Sn based solder need a full protection from corrosive solutions.

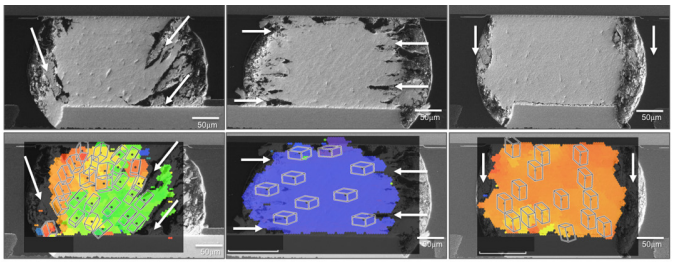

Figure 1. SEM images and OIM maps for 5% NaCl preconditioned joints showing how the corrosion attack is correlated with the Sn lattice basal planes. White arrows indicates the corrosion path [10].

Methods have been made to mitigate corrosive environment exposure to solder joints, using such solutions as conformal coatings. Systematic and in-depth studies had been reported and are still on going on protecting the systems and devices from external environmental risks, like corrosion, and their impact

to the component thermo-mechanical reliability were studied in various aspects [11-19]. Chen et.al reported the impact of conformal coating on BGA components under thermal cycling, vibration and drop test conditions and explained the correlation with the strain rate [13]. Yin et.al performed a study on conformal coated QFN components and reported that the coating reduce stress/strain in solder interconnects and constrains the out-of-plane deformation, which provided both positive and negative impact to the joint reliability [14]. It was also addressed that the level of coating material penetration under the component is an important consideration factor, which was also explained and analyzed in the publication by Serebreni et.al. [15]. Due to the coefficient of thermal expansion (CTE) mismatch, the loading condition per interconnect with and without conformal coating is often an important consideration factor. Detailed studies by Qi et.al and Tong et.al explore effects of the coating material thermo-mechanical behavior on PBGA and Ceramic packages, respectively, and addressed the coating material induced stress and strain impact [16,17]. Studies also reported conformal coating mitigating internally initiated defect risk, like Sn whisker, which can originate from the interconnect region towards outside, causing unexpected electrical shorts [18]. Overall, conformal coatings provide an effective approach of simple protection applied over board components in order to shield corrosion-prone electronic components from exposure. Various types of conformal coating polymer are offered commercially. These include acrylic, epoxy, urethane, silicone resin, and parlyne coatings with various mixed coating materials [19]. But as various earlier publications addressed, the stress and strain, induced from the coating material base properties, layer thickness and penetration under the component, are important consideration factors for a long-term reliability component interconnection. The study presented here is focused on the identification of the conformal coating layer induced strain and stress in the solder joints with various coating thickness, and to identify the effect of restriction of the loading conditions induced by the coating material with the combination of conformal coating and edgebond. A commercial ultra violet (UV) curable acrylated polyurethane conformal coating material was used in this study on 8x8mm² WLCSP components to effectively mitigate localized corrosion due to NaCl reaction. Spray coating applied partially coated components are compared to fully covered conformal coating configuration components, which variations are presented schematically in Figure 2. Ultra violet curing was performed using chemical reaction in the presence of high intensity UV light. A combination of edgebond and full covered conformal coating was tested to see a possible solution to enhance the thermal cycling performance. The extent of degradation, its microstructural evolution and possible mechanisms are discussed. To identify the strain and stress state per solder interconnect, electron backscattered diffraction (EBSD) analysis was performed using strain contour mapping and grain reference orientation deviation maps (GROD).

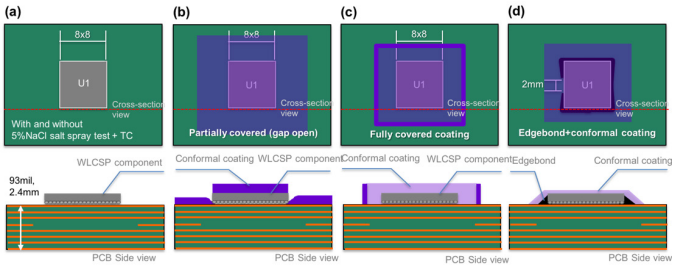

Figure 2. A schematic diagram of the WLCSP sample configurations. (a) assembled WLCSP without conformal coating, (b) Spray conformal coating applied sample configuration, (c) Fully conformal coated sample configuration and (d) Full edgebond with full conformal coating applied configuration.

EXPERIMENTAL PROCEDURE

Body size of 8x8mm², 0.4mm pitch wafer level chip scale package (WLCSP) with 250μm diameter Sn-4.0Ag-0.5Cu (wt%) (SAC405) solder balls were used in this study. A schematic diagram of the WLCSP sample configuration is shown in Figure 3. The parts were board-assembled on 2.4mm (93mil) high glass transition temperature (T_g), FR4-printed circuit boards with OSP surface finishes with a thermal profile of peak temperatures of 240°C, 60 seconds above the liquidus temperature. All components were assembled with SAC305 no-clean solder paste.

For conformal coating, UV curable acrylated polyurethane was used. The glass transition temperature (T_g) of the conformal coating material is -1°C with a coefficient of thermal expansion (CTE) of 122ppm/°C and 264ppm/°C, below and above the T_g, respectively. The coating was applied with spray coating process, which covered the whole PCB but remained partially open between the WLCSP edge and the PCB surface. As schematically shown in Figure 2(b), this allowed a small amount of NaCl solution to penetrate during salt spray testing. To prevent any open gap, the second configuration, a conformal coating dam was built around each component and filled with the conformal coating material to have a fully covered configuration (Figure 2(c)). The additional configuration with the combination of edgebond and conformal coating is presented in Figure 2(d). First, a reworkable edgebond adhesive was selected, which has a T_g of 130°C and a CTE of 30ppm/°C. To prevent voiding due to moisture releasing from PCB material during the curing cycle, test boards are pre-baked for 4 hours at 125°C. The edgebond adhesives were dispensed at room temperature using a pneumatic, hand-held dispenser. The board was then cured at 150°C for 30 minutes. The edgebond adhesive covered three full edges and one side-edge partially opened as indicated as an arrow in Figure 2(d).

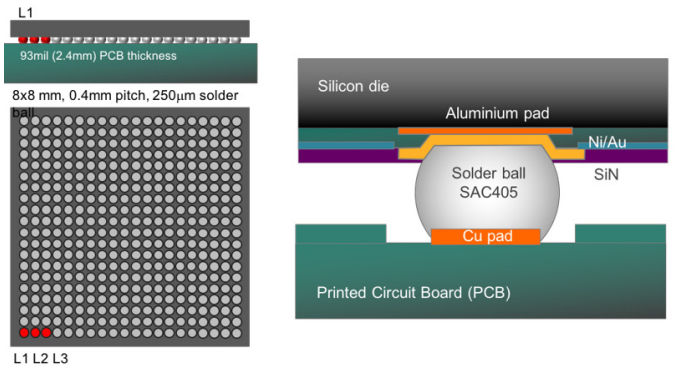

Figure 3. Wafer Level Chip Scale Package (WLCSP) Test component schematic configuration.

After assembly, all the test boards were treated in a salt spray environment with 5% sodium chloride (NaCl) aqua solution (or fog) at 35°C for 150 hours in an enclosed chamber. The salt spray test was performed based on the ASTM B117-09 standard but with an extended holding time for 150 hours instead of 96 hours. After the salt spray test, salt deposits were removed by a gentle rinse of deionized water at room temperature and dried in a dry chamber. For thermal cycling, samples were cycled from -40 to 125 °C at a ramp rate of 10°C per minute with 10 minutes of dwell time. A continuous resistivity measurement using data loggers was applied for each channel with in-situ monitoring during the test. The failure criterion in this study was based on the JESD22-A104D standard, a 20% increase of the peak resistivity for continuous five cycles relative to the initial value. Thermal cycling results for each condition were plotted as Weibull distribution plots.

Laser profilometer measurements were performed using a high accuracy linear displacement sensor (Keyence LK-H022) with a spot size of 25µm at reference distance of 20mm in conjunction with a heating stage designed for minimum z-axis movement during heating as shown in Figure 4. The heating stage was placed on a stepper motorized X-Y-Z stage. The laser sensor was protected from thermal effects with reflective shielding to maintain the operating temperatures of under 50 °C. Each Laser profilometer measurements were conducted at room temperature and 125 °C. As shown in Figure 4(a), each silicon die corner 0.5mm from the edge were measured for linear z-axis height comparison. For Full conformal coated samples, 0.5mm diameter drill holes are applied to measure the Si die top with the 25µm laser spot size.

Cross-sectional analysis using optical microscope with bright light and polarized light were applied to observe the evolution of the microstructures and the locations of the solder joint cracks. Electron microscopy and electron backscatter diffraction (EBSD) analysis was performed with a FEI Sirion FEG-SEM using oxford Instruments high speed EBSD detector. Oxford Aztec and Channel5 Tango software were used to index electron diffraction patterns and analyze collected EBSD data for grain boundary, inverse pole figure, strain contouring maps and grain reference orientation deviation (GROD) maps.

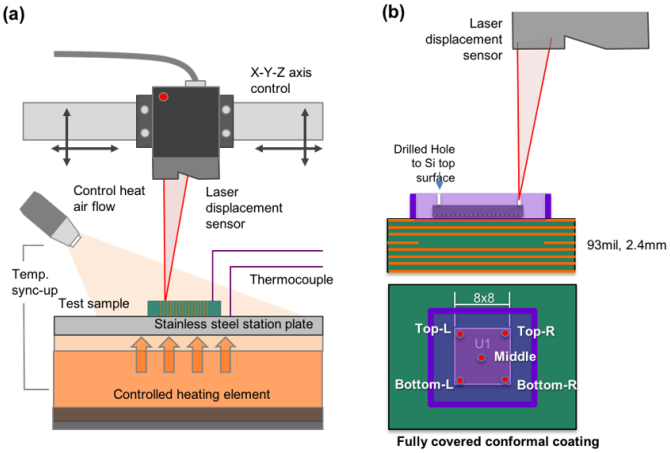

Figure 4. (a) Linear Laser height measurement schematic set-up and (b) sample laser measurement location.

RESULTS AND DISCUSSION

Figure 5 presents the Weibull plots of the thermal cycling results per sample configuration. The sample configuration without conformal coating, not treated with 5% NaCl shows a characteristic life cycle number of 404 cycles with a first failure at 354 cycles, where characteristic life cycle number is the cycle number at 63.5% failure rate. Compared to this baseline data set, the 5% NaCl salt spray treated samples show a characteristic life cycle number as 361 cycles, a small degradation of 10%. But comparing the first failure cycle between those two sample configurations, the cycle number for the NaCl salt spray treated sample component is 232 cycles compared to the no-NaCl treated samples, which is a significant 34% degradation. This can be explained by the corrosion mechanism, which do not affect all solder joint with an overall corrosion rate, but affects selected solder joint with preferred grain orientation, which are exposed to NaCl solution. Because of this, early impacted solder joints show localized corrosion areas causing earlier crack initiation, which led to shorter life cycle numbers. Compared to the no-coated samples, partially coated samples after NaCl treatment (Figure 2(b)), reveal a characteristic life cycle number of 367 cycles, which is similar to the NaCl salt spray treated samples. Also the first failure cycle number is similar with 276 cycles, compared to the NaCl treated samples without coating, which is only a marginal increase. This indicates that the coating layer provided little to no protection to the BGA joints, which is relatively obvious since there is an open gap between the WLCSP component edge and the PCB, so the NaCl solution can penetrate and cause damage to the BGA solder interconnects. Even though the penetration of NaCl solution is expected to be minimal, it can affect preferred Sn grain orientations and initiate the crack propagation.

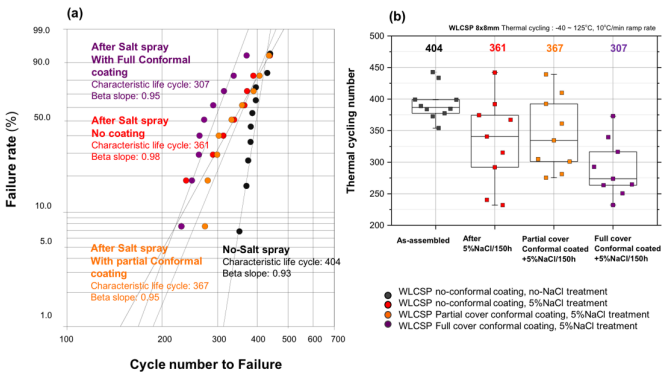

Figure 5. (a) Thermal cycling result Weibull distribution plot and (b) Thermal cycling Failure cycle number distribution plot per sample configuration and post-conditions.

Figure 6 shows the thermal cycled to failure corner solder joints per no-coating and partial coated components after NaCl treatment. As shown in Figure 6(a), as indicated in white boxes, corroded regions are observed at the surface of the solder joints and at the crack initiation region. The corner solder joint with partial conformal coating also show corroded regions at the surface and near the solder to package interface area, which accelerated the crack initiation, resulting in an accelerated crack propagation to failure. Unlike the partially coated samples, the fully coated samples did not show any evidence of NaCl solution penetration and corrosion reaction. But the characteristic lifecycle number is 307 cycles, which is even lower than the NaCl salt spray treated WLCSPs without any protection coating. Since it did not show any corrosion reaction at the BGA solder joints, the degradation seems to be caused by other factors, potentially by the conformal coating induced strain and stress. The cross section and SEM images are shown in Figure 7, comparing the no coating, no NaCl treated sample thermal cycled to failure sample to full conformal coated then thermal cycled sample solder joints. Each sample corner and two adjacent solder joints are selected and shown. Although all solder joints shown full crack propagation near the package side interface region, the non-coated WLCSP, after thermal cycling, exhibits crack propagation with a visually identifiable wide crack opening (Figure 7(a-c)). For the fully coated sample, after thermal cycling, Figure 7(d-f), the crack propagation is observed in a very tight and closed penetration path, which suggests that a compression stress was applied during the thermal cycling process. The height measurement between the package side interface and the board side Cu pad to solder interface before and after thermal cycling on fully conformal coated samples are shown in Figure 8 along with the no coated sample solder heights. As indicated in the full first row solder joints height distribution, a significant reduction of the solder height is identified.

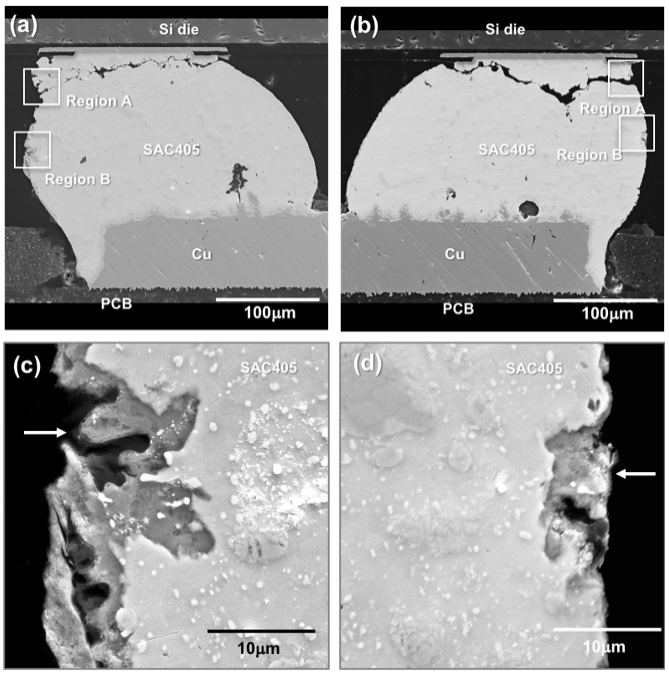

Figure 6. Scanning Electron microscopy (SEM) images on (a) (c) No conformal coating applied WLCSP and (b)(d) Partially conformal coated WLCSP after 5% NaCl spray test for 150h then thermal cycled to failure. Region A and B in (a) and (b) indicates the corroded region. (c) and (d) are higher magnification areas from Region B in (a) and (b). White arrows in (c) and (d)indicates the corroded regions.

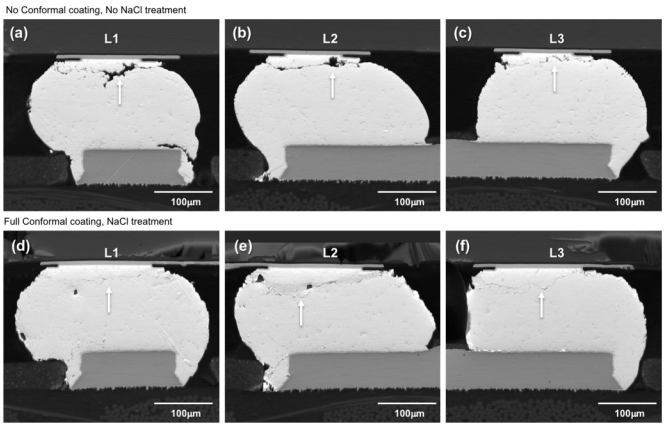

Figure 7. Scanning Electron Microscopy (SEM) images. (a) (b)(c) No conformal coating and no NaCl treatment applied WLCSP thermal cycled to failure,. (d)(e)(f) Full conformal coated samples after 5% NaCl spray test for 150h then thermal cycled to failure. Solder joint location indicated in Figure 2. (a)(d) corner solder joint, L1, (b)(e) L2 and (c)(f) L3. White arrows indicates the crack location.

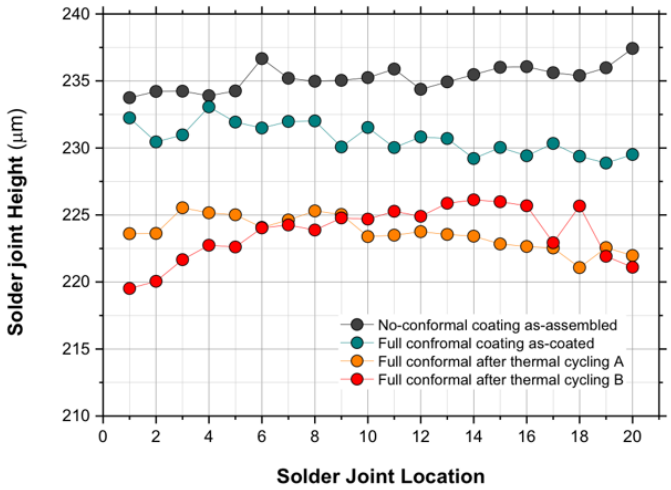

Figure 8. Solder joint height variation per component configuration and thermal cycling.

The reason for the height reduction induced constant compression strain, during thermal cycling can be explained from the component cross-section shown in Figure 9. The coating dam surrounded the WLCSP and the conformal coating material was applied to fill inside the dam to have a full conformal coating configuration. The overall thickness of the conformal coating is 1.3mm, which is 380μm on top of the WLCSP component top surface. Even though this coating is not optimized for best practice, since thinner coating layer is preferred, the coating provided a high level of corrosion protection. Volume shrinkage of the conformal coating materials with long term elevated temperature exposure potentially affected the solder height during thermal cycling, which apply compression stress and strain to the solder interconnects. But the reduction in solder height and compression strain cannot be the dominant factor for the shorter characteristic life cycle numbers, since compression strain to each solder joint actually enhance the solder stability and mitigate the crack initiation and propagation and, should actually result in a longer lifecycle performance, which contradicts the results shown in Figure 5. To identify any possible factor, a linear laser height measurement was applied to Fully conformal coated WLCSPs comparing the height at room temperature and at 125°C. The measurement locations are indicated in Figure 4(a) and the results are shown in Figure 10.

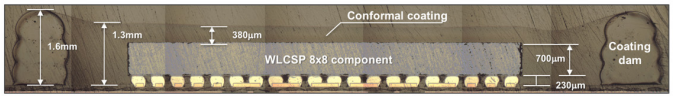

Figure 9. Fully conformal coated WLCSP side view cross section optical image

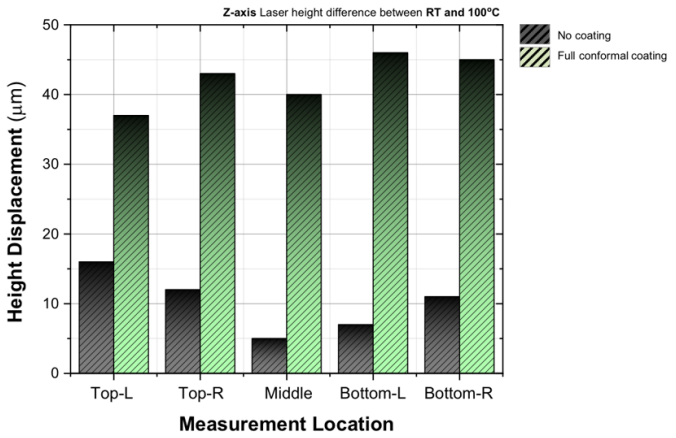

Figure 10. Linear Laser height displacement measurement comparison between room temperature and 125oC for no conformal coated WLCSP and fully conformal coated WLCSP. Laser measurement location are indicated in Figure 4(b).

The height difference between room temperature and 125°C for no conformal coated WLCSP are in the range of 6μm (middle) to 16μm (top left corner). Relative to the middle point, the corner region show a slightly higher height difference. But for the fully conformal coated sample, the Si die surface height difference indicated a 37μm (top left) to 47μm (bottom left) rage of displacement at 125°C, which confirms that the at higher temperature a tension strain induced and negatively affects the stability of the solder joints in fully coated components. The electron backscattered diffraction (EBSD) analysis also revealed the straining in fully coated component solder joint as shown in Figure 11. Three solder joints per no coated and fully coated components shown in Figure 7 are EBSD scanned and each inverse pole figure (IPF), strain contour and grain reference orientation deviation (GROD) maps are compared. Based on the IPF images in Figure 11(a), the no coated component solder joints maintained their single to dual grain structures and developed localized fine grain and recrystallized structure near the package side interface where crack propagation occur. Compared to fully coated component solder joints in Figure 11(b), an overall fully distributed grain refinement is observed with a dominant refinement in L1 joint. The associated strain contour maps revealed a well distributed high level of strain, which can be compared to the low level of strain distribution in no coating applied component solder joints. The strain contour map is converted from scanned EBSD information based on local misorientation and can identify the localized grain region, which measures the level of deviation from the theoretical, non-strained lattice, revealing a distribution map of relatively higher plastic deformation regions [20]. The GROD map in comparison reveals indirectly the relative residual stress level compared to the adjacent grain, by revealing the level of tilting per individual grain compared to a grain orientation reference [20]. Comparing the two EBSD scanning based information conversion, the relative

level of strain and stress for each solder joint can be analyzed. In Figure 11(a) the L1 joint has an overall lower level of strain but localized strain is detected near the package side interface with a relatively high residual stress. But compared to the no coated component L1 joint, the L1 joint in the fully coated component, reveal a full solder high strain level with less residual stress, which means it experience not only a shearing but also an overall tension and compression in the Z-axis direction.

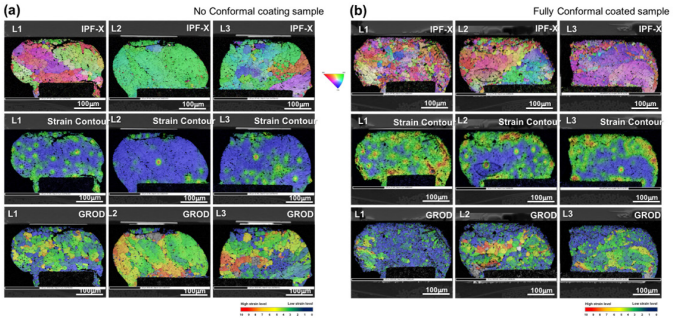

Figure 11. Electron Backscattered Diffraction (EBSD) images for (a) No conformal coated WLCSP after thermal cycling to failure and (b) Fully conformal coated WLCSP after 5% NaCl salt spray test and thermal cycling to failure. The SEM images for L1 to L3 solder joints per sample configuration are shown in Figure 7. Top row is the inverse pole figure (IPF) images, the middle row is the strain contour map, and the bottom row is the Grain reference orientation deviation map.

The EBSD analysis comparison results of these two solder joints, aligned with the laser measurement result and the crack opening comparison in Figure 7. Increased lattice strain in fully conformal coated sample alludes to increased applied strains to the joint by the addition of conformal coating. Recrystallization due to stress relaxation during thermal cycling results in the observed reduction in grain size across the failed joints. The joints from the conformal coated samples revealed increased distribution of recrystallized area per solder joint, which is observed across a majority of the solder joints. This is due to an increased magnitude of thermo-mechanical strain applied by the conformal coating on the joints through large CTE mismatch between the component and PCB. For non-conformal coated samples, recrystallized section of the joints are more localized within the joint, indicating less thermo-mechanically induced strains during thermal cycling. Examining the conformal coating material, the conformal coating shares characteristics of a coefficient of thermal expansion (CTE) of 264 ppm/ °C above a glass transition temperature of -1°C. Compared to average FR4 values of 16-20 ppm/ °C and a glass transition temperature of 135°C. These characteristics indicates that the conformal coating has a greater displacement change with temperature than the FR4 PCB material. Strains generated by the conformal coating on the solder joints are expected with this CTE mismatch between the package assembly and the conformal coating. To find a possible solution to the corrosion and mechanical stress driven degradation, a combination of edgebond and conformal coating was considered and tested. As shown in Figure 2(d), a reworkable edgebond material was applied before conformal coating. The coating covered the edgebond, which closed the gap between the WLCSP and the PCB. Thermal cycling results are shown in Figure 12. The Weibull plot depicts the reliability of the fully conformal coated WLCSP against the edgebond with conformal coated WLCSP. Characteristic life cycle numbers of the edgebond with conformal coated WLCSP was 2784 cycles. The use of edgebond in conjunction with a spray-on conformal coating improved thermal cycling characteristic life by 909% compared to a full conformal coated sample, and 588% improvement over non-coated WLCSP exposed to 150 hr 5% NaCl salt spray test. First failure cycle number was also improved by a similar margin.

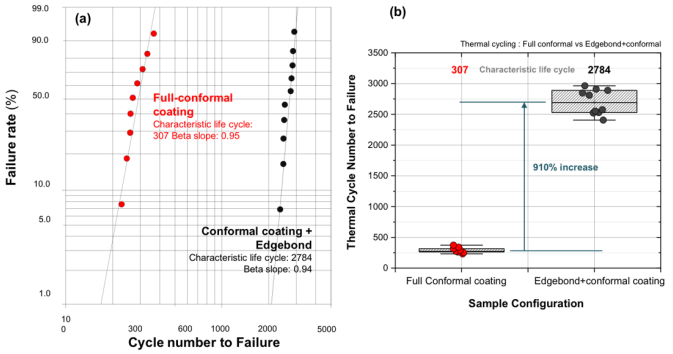

Figure 12. Comparing Fully conformal coated WLCSP with and without Edgebond (a) Thermal cycling result Weibull distribution plot and (b) Thermal cycling Failure cycle number distribution plot per sample configuration.

The mechanical and thermal performance enhancement using edgebond adhesive was studies in various applications [21-24]. Securing the corner and edge without affecting the solder BGA often resulted in an vast improvement in dynamic shock and bend conditions, and with the right combination of T_g and CTE the adhesive improves the thermal cycling performance in both small components like WLCSPs and large components like FCBGAs [21,24]. The main role of these edgebond adhesive is the mitigation of the thermo-mechanically induced strain at the corner and edge region of the component, which resulted in a more stable structure. The combination of edgebonding and conformal coating, which is presented here, provided the enhancement of the thermal cycling performance by restricting the conformal coating induced strain, identified via z-axis height measurement and microstructure EBSD analysis. Thus, the combination of edgebond and conformal coating provides both corrosion resistance and enhanced thermo-mechanical stability to the component.

CONCLUSION

Every day integration of electronic devices requires corrosion resistant methods to be employed in order to maintain device reliability. With this in mind, industry offerings of conformal

coatings provide an option to fulfill that requirement. Conformal coating application methods must be taken into consideration when choosing the method of applying conformal coatings. This allows the prevailing failure mechanism to be dictated by corrosion on the joints, shown through Weibull plots demonstrating similar device characteristic life to that of the non-coated components. However, despite full coverage with conformal coating against corrosion, a new failure mechanism is introduced which supersedes corrosion impacts. The fully coated samples show no evidence of corrosion but show degraded thermal cycling performance due to the coating induced compression stress. The coefficient of thermal expansion mismatch between the conformal coating and the WLCSP can negatively impact device thermal cycling performance. In this case, possible coefficient of thermal expansion to the Z-axis direction serves as a driving force, which amplifies applied strain on the interconnects leading to reduced interconnect characteristic life and initial failure cycle count. Potential resolution to this is offered in the form of edgebond adhesive application. A combination of edgebond with conformal coating provides the full benefits of corrosion resistance while improving device reliability.

ACKNOWLEDGEMENTS

This work is a research project supported by Zymet and Cisco Component Quality and Technology group.

REFERENCES

1. M. Abtew, G. Selvaduray, Mater. Sci. Eng. R 27, 95 (2000)

2. D. Frear, H. Morgan, and J.H.Lau, eds. The Mechanics of Solder Alloy Interconnects, (New York: Van Nostrand Reinhold, 1994)

3. H.G. Song, J.W. Morris Jr., F. Hua, JOM 56, 30 (2002)

4. Bo Liu, Tae-Kyu Lee, and Kuo-Chuan Liu, J. Electron. Mater. 40(10), 2111 (2011)

5. A.J.Hale and H.S.Fosteh, J.Soc.Chem.Ind. 9, 2371 (1915)

6. A.Jermstad and A.Gaule, J.Inst. Met. 13, 1370 (1919)

7. B.Y.Wu, Y.C.Chan, and M.O.Alam, J.Mater.Res. 21(1), 62 (2006)

8. D.Li, P.Conway, and C.Liu, Corrosion Sci. 50, 995 (2008)

9. J.Y.Jung, S.B.Lee, H.Y.Lee, Y.C.Joo, and Y.B.Park, J. Electron. Mater. 37(8), 1111 (2008)

10. Tae-Kyu Lee, Bo Liu, Bite Zhou, Thomas Bieler and Kuo-Chuan Liu, J. Electron. Mater. 40(9), 1895 (2011)

11. P.Zhao and M.Pecht, IEEE Trans. on Device and Mat. Rel. 5(2), 268 (2005)

12. K.Kokko, L.Frisk and P.Heino, Soldering and Surface mount technology 22(3), 42 (2010)

13. D.Chen and M.Osterman, Proceeding of the IEEE Accelerated stress testing and reliability conference, Pensacola Beach, FL, (2016)

14. C.Yin, S.Stoyanov,C.Bailey, and P.Stewart, IEEE Trans. on Component, Packaging and Manufacturing Technology 9(11), 2210 (2019)

15. M.Serebreni, R.Wilcoxon, D.Hillman, N.Blattau, and C.Hillman, Proceeding of the 33rd Thermal measurement, Modeling and Mahangement Symposium, San Jose, CA, 40(2017)

16. H.Qi, M.Osterman, and M.Pecht, IEEE Trans. on Electronic Packaging Manufacturing 32(1), 32(2009)

17. H-.M.Tong, L.Mok, K.Grebe, H.Yeh, K.Srivastava, and J.Coffin, IEEE Trans. on Components, Hybrids and manufacturing technology 16(5), 571(1993)

18. S.Han, M.Osterman, S.Meschter, and M. Pecht, J. Electron. Mater. 41(9), 2508 (2012)

19. B. Medgyes and G. Ripka, IEEE proceedings 30th International Spring Seminar on Electronics Technology (ISSE), Romania, May, 429 (2007)

20. S.Wright, N.Nowell, and D.Field, Microscopy and Microanalysis, 17(3), 316 (2011)

21. H.Wu, F.Song, J.Lo,T.Jiang, K.Newman, and R.Lee, Proceeding of 59th Electronic Components and Technology Conference, San Diego, CA, 125 (2009)

22. B. Toleno and J. Schneider, Proceedings of 28th Int. Electron. Manuf. Technol. Symp., San Jose, CA, 299 (2003)

23. K. Meyyappan, A. McAllister, M. Kochanowski, and I. Hsu, IEEE Transactions on Components and
Packaging Technologies, 31(3), 670 (2008)

24. S. Perng, T-.K. Lee, and C. Guirguis, Proceedings of SMTA International, Rosemont, IL, 375 (2013)